AIMS Energy, 11(6): 1231–1251.
DOI: 10.3934/energy.2023056
Received: 26 July 2023
Revised: 13 October 2023
Accepted: 19 October 2023
Published: 23 November 2023

http://www.aimspress.com/journal/energy

Research article

A novel monotonic wind turbine power-speed characteristics model

Al-Motasem Aldaoudeyeh[1], Khaled Alzaareer[2], Di Wu[3], Mohammad Obeidat[1], Salman Harasis[1], Zeyad Al-Odat[4,*] and Qusay Salem[5]

[1] Department of Electrical Power and Mechatronics Engineering, Tafila Technical University, Tafila, Jordan

[2] Energy Engineering Department, Al Hussein Technical University, Amman, Jordan

[3] North Dakota State University, North Dakota, USA

[4] Department of Computer and Communications Engineering, Tafila Technical University, Tafila, Jordan

[5] Department of Electrical Engineering, Princess Sumaya University for Technology, Amman, Jordan

* **Correspondence:** Email: zeyad.alodat@ttu.edu.jo.

Abstract: Major issues with logistic functions (LFs) in modeling wind turbine power-speed characteristics (WTPSCs) include: 1. low accuracy near cut-in and rated wind speeds due to lack of continuity; 2. difficulties in fitting their parameters because of ill-conditioning; 3. no guaranteed monotonicity; 4. no systematic way to determine upper and lower limits for their parameters. The literature also reports that six parameter LFs may sometimes provide less accurate results than five, four, and three parameter models, implying: 1. they are unsuitable for WTPSC modeling; 2. lack of systematic method to determine upper and lower limits for optimization algorithms to search in. In this paper, we propose a new six parameter LF then employ subspace trust-region (STIR) algorithm to estimate its parameters. We compare the accuracy of our six parameter model to others from the literature. With 42 on-shore and off-shore WTs database of ratings varying from 275 to 8000 kW, we the comprehensiveness of our model. The results show an average mean absolute percent error (MAPE) of 2.383×10^{-3}. Furthermore, our model reduces average and median normalized root mean square error (NRMSE) by 32.3% and 38.5%, respectively.

Keywords: logistic functions; wind turbine power curve; parametric models; parameters estimation; subspace trust region

Abbreviations: DE: Differential evolution; EA: Evolutionary algorithm; EP: Evolutionary programming; GA: Genetic algorithm; GCR: Generator control region; GWEC: Global wind energy council; LF: Logistic function; LSE: Least-Square error; MAE: Mean absolute error; MAPE: Mean

absolute percent error; NRMSE: Normalized root mean square error; PDF: Power distribution function; PSO: Particle swarm optimization; RMSE: Root mean square error; STIR: Subspace trust-region; TI: Turbulence intensity; WT: Wind turbine; WTPSC: Wind turbine power-speed characteristics; SDS: Significant downwards shifting; SUS: Significant upwards shifting; MDS: Minor downwards shifting; MUS: Minor upwards shifting; CBS: Curve becomes steeper; CBF: Curve becomes flatter; NDS: Negligible downwards shifting; NUS: Negligible upwards shifting; DbS: Decrease (in $q(\vec{\theta}, v)$) by horizontal shifting; IoD: Increase or decrease (in $q(\vec{\theta}, v)$) by horizontal shifting

1. Introduction

WT installations experienced an unprecedented annual growth of 53 % in 2020. GWEC reports that, with 93 GW of new installations in 2020, the global cumulative capacity reached 743 GW [1].

Such growth is attributed to factors such as: 1. innovations in blades design and fabrication [2]; 2. improvement in nacelle components reliability (e.g., gears with fatigue and wear resistance and new softwares for system level modeling of the nacelle) [2]; 3. improved sensors and control algorithms [2]; 4. political support (e.g., low carbon energy goals, feed-in tariffs, or guaranteed access to the transmission grid) [3, 4].

WTPSCs play significant roles in: 1. risk assessment [5]; 2. wind energy yield and WT selection [5]; 3. condition monitoring [6]; 4. sizing storage capacity for wind power integration [7]; 5. predictive control optimization [8]; 6. WTs troubleshooting [8]; 7. detection of degradation because of aging [6]; 8. optimal dispatching of wind farms [6].

Near cut-in wind speed, WTPSCs are difficult to model [9]. Although we theoretically expect WTs power to exhibit a cubic relationship with wind (when it is below rated speed), this is incorrect. The conversion efficiency of WTs varies with speed, which is most remarkable near cut-in and rated wind speeds. Just slightly above cut-in speed, virtually all WTs exhibit a steep growth in efficiency. Near rated wind speeds, WTs 'spill' wind energy [10], decreasing the efficiency. The result is complex and nonlinear relationship between wind speed and the WT power output [11].

The general shape of LFs (sometimes referred to as logistic distributions or activation functions) made them meaningfully suitable for scientific modeling of bacteria and plant growth since a growing population 'competes' for resources, placing an upper limit on the number of bacteria/plants [12]. LFs can also be useful for certain biological, chemical, linguistic, political science topics [13].

Since both of LFs and WTPSCs are 'S'-shaped, LFs are (at least in principle) candidates for accurate WTPSC mathematical models. LFs are parametric models (they are based on mathematical expressions with a fixed number of parameters), bringing potential to offer some analytical advantages. For instance, in wind energy assessment, it is possible to use them along with Weibull distribution to obtain explicit PDFs [14]. Lydia et al. [15] are among the earliest researchers to attempt modeling WTPSCs curves using LFs. They propose a 5-parameter LF and estimate its parameters using GA, EP, PSO and DE. Many researchers have sought new methods to estimate the parameters of the LF proposed by Lydia et al. [15] (e.g., [6, 16, 17]). Sohoni et al. [9] reported that certain LFs (due to explicitly including an inflection point in their parameters) have the potential to increase accuracy and improve online-monitoring using LFs. Pei and Li [11] confirmed this by parameterizing various WTPSC models and comparing them using statistical metrics, such as MAE and RMSE.

Jing et al. [18] improved the model of Lydia et al. [15] by introducing 'quantile dependency' to its parameters. Jing et al. [18] parameterized the model proposed by Lydia et al. [15] using PSO for three wind farms and validating the accuracy of their work using MAPE and NRMSE.

Villanueva and Feijóo [19] proposed two 'generalized' 6-parameter LFs and estimate their parameters using evolutionary optimization techniques. The proposed models show substantial accuracy improvement, but Villanueva and Feijóo [19] reported difficulties in optimizing their parameters.

Zou et al. [17] reviewed three, four, five, and six parameter LFs and their accuracy using MAE and RMSE. Results show that six parameter LF may sometimes provide lower accuracy than four and three parameter LF. Thus, adding new parameters to LFs does not necessarily contribute to increased accuracy. Villanueva and Feijóo [19] reported similar results.

In Section 2, we provide a mathematical background on WTPSC and LFs and highlight their limitations and our contributions. Section 3 proposes a new LF model, demonstrates its curve fitting merits, and develops upper and lower limits on its parameters. We validate our model in Section 4 by providing graphical and numerical accuracy results. To ensure a suitable comparison, we compare our work with other 6-parameter LFs. Section 5 draws final remarks, discusses the limitations of the study and puts forth suggestions for future investigations. A summary of the literature gap and the most significant contributions are then mentioned in Section 6.

2. Background and contribution summary

2.1. Mathematical representation of WTPSC

For stall or pitch-controlled WT, it is possible to characterize the WTPSC curves mathematically as [5]

$$P_{e,WT}(v) = \begin{cases} 0 & v < v_{ci} \\ q_e(\vec{\theta}, v) & v_{ci} \leq v \leq v_r \\ P_r & v_r < v \leq v_{co} \\ 0 & v > v_{co} \end{cases} \tag{1}$$

where v is the wind speed. v_{ci}, v_r, and v_{co} are the cut-in, rated, and cut-out speeds of the WT, respectively. P_r is the rated output power of the WT. $q_e(\vec{\theta}, v)$ is a mathematical expression which should (ideally) accurately estimate the manufacturer-provided data (i.e., empirical power-speed pairs in the GCR). Such estimation is typically done by fitting a vector of parameters $\vec{\theta}$ using the least-squares method [5].

2.2. Preliminary concepts

Figure 1 depicts a WTPSC curve. When estimating $\vec{\theta}$ parameters to fit the manufacturer datasheet, some points of interest assist us in establishing its limits.

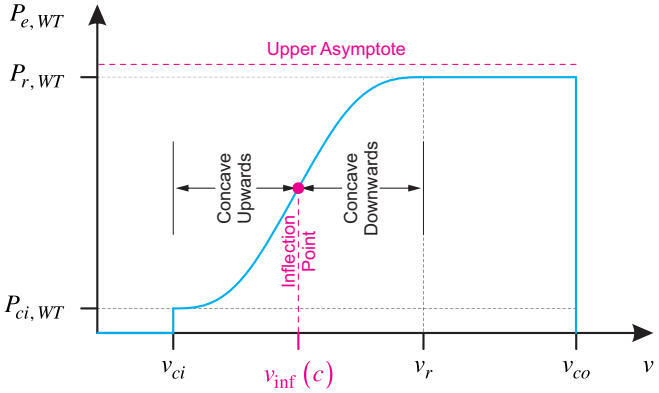

Figure 1. WTPSC with inflection point and upper asymptote.

1. The curve is monotonic. This means it always increases (or at least remains the same) with v. Mathematically, this means the first derivative must remain greater than or equal to zero, as Eq 2:

$$\frac{d\,q_e(\vec{\theta}, v)}{d\,v} \geq 0, \quad \forall\, v \geq 0 \tag{2}$$

2. For virtually all WTPSC curves, an inflection point exists. This is the point at which the curve switches from *concave upwards* to *concave downwards*. Mathematically, this means the second derivative must be zero, as Eq 3:

$$\left.\frac{d^2\,q_e(\vec{\theta}, v)}{d\,v^2}\right|_{v=v_{\inf}} = 0 \tag{3}$$

   Where $v_{\inf}$ is the inflection point.

3. One major attribute of LFs is that they should approach an upper asymptote when their dependent variable approaches infinity. Mathematically, this means

$$\lim_{v\to\infty} q_e(\vec{\theta}, v) \approx P_{r,WT}$$

   Ideally, the upper asymptote of WTPSC should be close to P_r. This trend of approaching an upper asymptote is obvious in virtually all WTPSC curves when $v \to v_r$. In practice, v is never ∞, but this mathematical formulation benefits in establishing upper and lower limits for $\vec{\theta}$ parameters, which, in turn, assists the optimization algorithm by searching in a suitable region instead of arbitrarily determining it by trial and error.

2.3. Limitation of previous methods and summary of contribution

6-parameter LFs are discussed in Villanueva and Feijóo [19] and have one of the following forms

$$q(\vec{\theta}, v) = d + \frac{a-d}{\left(\varepsilon + \left[\frac{v}{c}\right]^{-b}\right)^{g}} \qquad \text{6PL} \tag{4}$$

$$q(\vec{\theta}, v) = d + \frac{a-d}{\left(\varepsilon + \mathrm{e}^{-b\,(v-c)}\right)^{g}} \quad \text{6PLE} \tag{5}$$

where a and d are the upper and lower asymptote, respectively. b is the growth rate (sometimes called 'hill slope') around point c. g is called the 'asymmetry factor' because it tunes the degree of asymmetry around point c [11, 15]. c is the inflection point (the point at which $q(\vec{\theta}, v)$ turns from concave upward to concave downward). ε has no special meaning, but has a value around one [8].

Disadvantages of fits in Eqs 4 and 5:

1. With some WTs, they inaccurately fit the WTPSC, especially near v_{ci} and v_r. This is reported by as a disadvantage for piecewise models, which is the conventional way to account for the effect of turning off the WT when $v < v_{ci}$ and $v > v_{co}$ [9]. Yan et al. [20] reports such inaccuracy for LFs even with continuous WTPSC;

2. Contain a high number of parameters compared to other fits with fewer parameters, but better accuracy. For example, Zou et al. [17] review three, four, five, and six parameter LF and tested their accuracy using MAE and RMSE. Results showed that 6-parameter LF may sometimes provide lower accuracy than three, four and five parameter LFs. Pei and Li [11] report similar results. Thus, adding new parameters does not contribute to increased accuracy. Intuitively, adding new parameters should provide certain advantages, such as accuracy improvement;

3. Their monotonicity is not guaranteed when the parameters are estimated using EAs. We overcome this disadvantage in Aldaoudeyeh et al. [8];

4. Sometimes LFs have the possibility of becoming ill-conditioned, making the estimation of $\vec{\theta}$ parameters difficult [9].

This paper contain the following contributions:

1. We propose a new 6-parameter LF model for WTPSC curves; 2. We develop constraints on the parameters of our model to guarantee its monotonicity; 3. The model exhibits excellent fit that is at least as accurate as 6PL and 6PLE for some WTs, but also provides significant MAPE and NRMSE improvements. It also provides high accuracy near v_{ci} and v_r; 4. The parameters of our model are easily optimized with the STIR algorithm.

3. The proposed model

Our proposed model is

$$q(\vec{\theta}, v) = d + \frac{a-d}{\left(1 + \left[\frac{v}{c}\right]^{\zeta} \mathrm{e}^{-b\,(v-c)}\right)^{g}} \tag{6}$$

where a is the upper asymptote. d is a parameter to tune the lower asymptote near v_{ci} (i.e., d is not the lower asymptote, but it drastically influences it). b is the growth rate around point c. g is called the 'asymmetry factor' because it tunes the degree of asymmetry around point c. c is the inflection point. ζ is the steepness tuning factor.

We call this model 6PLEZ. At a glance, 6PLEZ model resembles 6PL and 6PLE (Eqs 4 and 5), but, as we will see in Section 4, it is more accurate. To our best knowledge, the literature does not contain this model. Villanueva and Feijóo [21] and Zou et al. [17] review WTPSC models (including LFs models), but the 6PLEZ model does not appear on any of them.

We estimate $\vec{\theta}$ parameters with the same method mentioned in Aldaoudeyeh et al. [8] (LSEs objective function minimized using STIR algorithm).

3.1. Characteristics of the 6PLEZ model

In this subsection, we illustrate the effect of $\vec{\theta}$ parameters variation on $q(\vec{\theta}, v)$ shape. Unless otherwise is specified, the parameters are $a = 1$, $b = 1.25$, $c = 6$, $d = 0$, $g = 1$, and $\zeta = 0$. The dependent parameter (v) is shown from 2.5 (typical v_{ci}) to 12 (typical v_r).

Figure 2 shows the effect of varying a and d on the shape of $q(\vec{\theta}, v)$. Clearly, increasing a slightly shifts the curve upwards near v_{ci}. This effect becomes more pronounced the closer we get to v_r, where the upper asymptote varies linearly with a. The final value of $q(\vec{\theta}, v)$ is a. We thus call it the upper asymptote. We also note that increasing a steepens the curve near c.

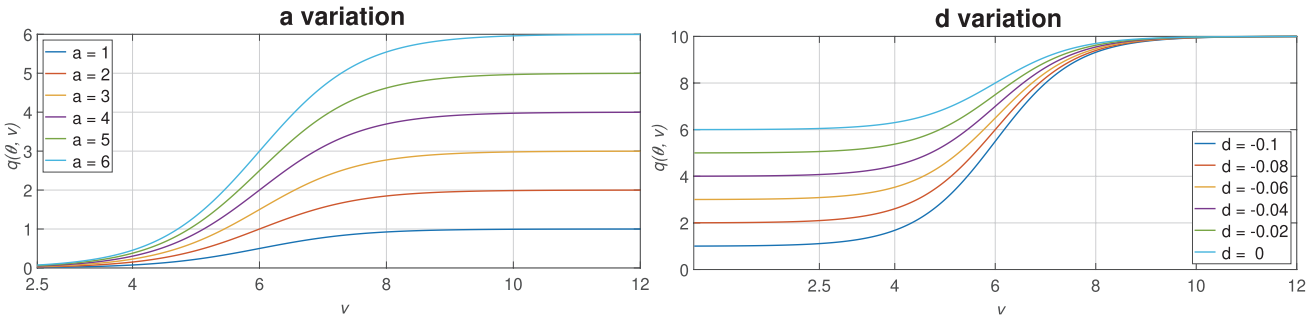

Figure 2. Effects of a and d on the shape of $q(\vec{\theta}, v)$.

The effect of d is better illustrated with $a = 10$ and when we extend the curve from 0 to v_r. Increasing d shifts the upwards curve near v_{ci} and its effect diminishes at v_r. We also note that increasing d flattens the curve near c.

Thus, most of a and d effect is to *scale* the maximum and minimum asymptotes of the LF curve, respectively. By contrast, b, c, g, and ζ (as we will discuss now) *define the shape* of the LF.

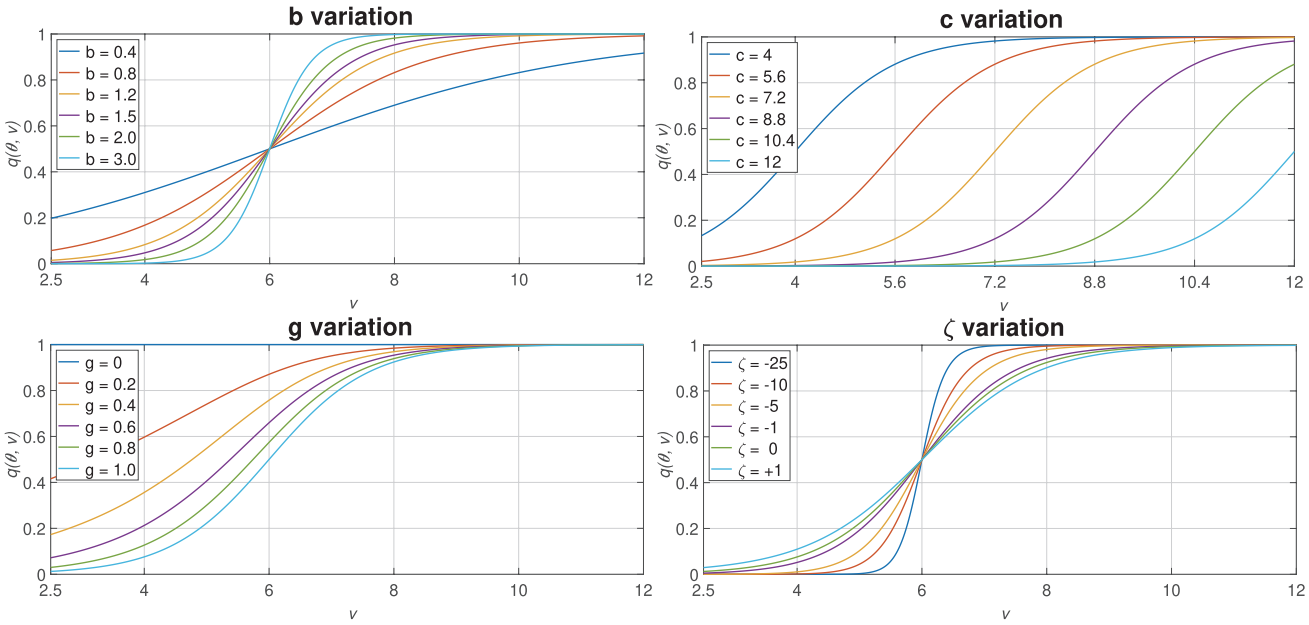

Figure 3. Effects of b, c, ζ, and g on the shape of $q(\vec{\theta}, v)$.

Figure 3 shows the effects of b, c, g, and ζ variation on $q(\vec{\theta}, v)$ shape. The increase in b shifts the curve downwards near v_{ci} and upwards near v_r. However, it is also obvious from the curve that the effect is more pronounced near v_{ci}. As b increases, the curve becomes steeper near the inflection point ($v_{\text{inf}} = c$).

The variation of c only shifts the curve to the left and right. In fact, it is worth mentioning that all curves for varying c are the same, but merely shifted horizontally. It is possible to conclude from Figure 3 that increasing c decreases $q(\vec{\theta}, v)$ near v_{ci}, and increases or decreases $q(\vec{\theta}, v)$ near v_r.

The increase in g drastically downshifts the curve near v_{ci}. It also substantially downshifts the curve near v_{inf} and makes it steeper, but has no effect on the power curve near c. As we increase ζ, $q(\vec{\theta}, v)$ shifts slightly upward and becomes flatter near c, but has no effect on $q(\vec{\theta}, v)$ near v_r. In a sense, ζ adjusts the steepness around c while having a negligible effect minor increase effect v_{ci} and a negligible decrease near v_r.

Note that b and ζ seem to provide the same effect. Remarkable differences, however, are: 1. b tunes the steepness while having significant effect near v_{ci} and a minor effect near v_r; 2. ζ tunes the steepness while having minor effect near v_{ci} and a negligible effect near v_r.

Table 1. Effects of $\vec{\theta}$ parameters near important points on WTPSC curve.

Parameter	v_{ci}	v_{inf}	v_r	Notes
a	MUS	SUS	SUS	the upper asymptote as $v \to \infty$
b	SDS	CBS	MDS	
c	DbS	IoD	IoD	shifts the curve horizontally while the shape remains the same
d	SUS	SUS	NUS	
g	SDS	CBS	NDS	
ζ	MUS	CBF	NDS	

Table 1 shows a summary of the previously mentioned effects. In Figure 4, we list some examples on why our model provides higher accuracy. The dashed lines show curves with low accuracy in some region and the high accuracy in others, while solid lines are improvements due to variations in $\vec{\theta}$. Circles are manufacturer-provided data.

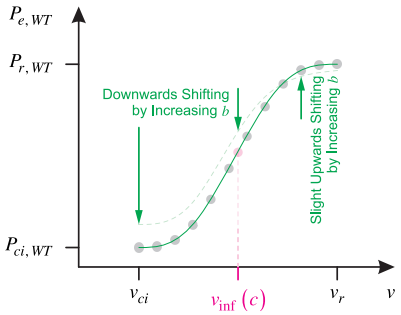

(a) Example of varying b to enhance fitting near v_{ci} and $v_{\inf}$ (Note the minor effect near v_r)

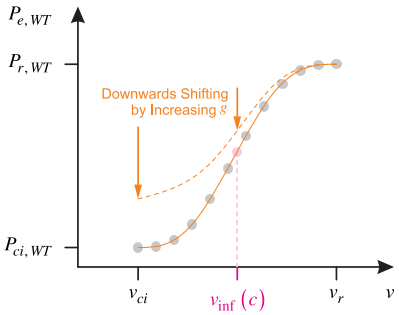

(b) Example of varying g to enhance fitting near v_{ci} and $v_{\inf}$ (Note the absence of effects near v_r)

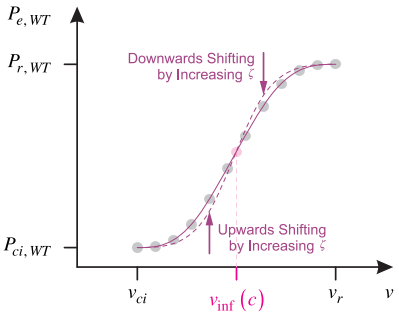

(c) Example of varying ζ to enhance fitting to the left and right of $v_{\inf}$ (Note the minor effects near v_{ci} and v_r)

Figure 4. Examples on 6PLEZ model flexibility.

In Figure 4a, we see low accuracy near v_{ci} and $v_{\inf}$. The error is positive and tends to decrease the closer we get to v_r, but turns negative at v_r. In this case, increasing b substantially increases the accuracy since it shifts the curve downward near v_{ci}, moderately downward near $v_{\inf}$, and slightly shifts the curve upward near v_r. In Figure 4b, we see a case where substantial errors occurring near v_{ci} but they disappear as the speed increases and accuracy is very high near v_r. A suitable solution is to increase g, which shifts the curve downward with larger shifting occur closer to v_{ci}, but no effect at v_r. Figure 4c shows a curve providing high accuracy near v_{ci} and v_r. The error, however, to the left/right of $v_{\inf}$ is negative/positive, with a slope greater than the slope of manufacturer-provided data. In this case, increasing ζ improves the accuracy by flattening the curve near $v_{\inf}$.

The previously mentioned examples demonstrate the flexibility of the 6PLEZ model and why it provides significant accuracy improvements. *Our model adapts to improving the accuracy in some regions (near v_{ci}, $v_{\inf}$ or v_r) without sacrificing the accuracy in the others.*

3.2. Constraints on the proposed six-parameter LF (6PLEZ)

In this section, we devise some limits on the 6PLEZ model parameters (Eq 6), which help the STIR algorithm minimize the objective function (i.e., LSEs). We define the main limits on $\vec{\theta}$ as (the subscripts min and max denote the minimum and maximum limits of each parameter, respectively)

$$\begin{aligned} a_{\min} \le a \le a_{\max}, \quad & b_{\min} \le b \le b_{\max} \\ c_{\min} \le c \le c_{\max}, \quad & d_{\min} \le d \le d_{\max} \\ g_{\min} \le g \le g_{\max}, \quad & \zeta_{\min} \le \zeta \le \zeta_{\max} \end{aligned}$$

3.2.1. Monotonicity conditions

To guarantee increasing monotonicity, the derivative of $q(\vec{\theta}, v)$ must be positive or zero. Thus, differentiating Eq 6 we get

$$\frac{g\left[b\left[\frac{v}{c}\right]^{\zeta} \mathrm{e}^{-b(v-c)} - \frac{\zeta\left[\frac{v}{c}\right]^{\zeta-1}\mathrm{e}^{-b(v-c)}}{c}\right](a-d)}{\left(1+\left[\frac{v}{c}\right]^{\zeta}\mathrm{e}^{-b(v-c)}\right)^{g+1}} \geq 0 \qquad \forall v \geq 0 \tag{7}$$

Equation 7 can be simplified as

$$\frac{g\left[\left[\frac{v}{c}\right]^{\zeta} \mathrm{e}^{-b(v-c)}(bv-\zeta)\right](a-d)}{v\left(1+\left[\frac{v}{c}\right]^{\zeta}\mathrm{e}^{-b(v-c)}\right)^{g+1}} \geq 0 \qquad \forall v \geq 0 \tag{8}$$

The inequality of Eq 8 is satisfied when

$$\begin{array}{ll} a \geq d & \text{Monotonicity Condition 1} \\ b \geq 0 & \text{Monotonicity Condition 2} \\ c \geq 0 & \text{Monotonicity Condition 3} \\ g \geq 0 & \text{Monotonicity Condition 4} \\ \zeta \leq b v_r & \text{Monotonicity Condition 5} \end{array}$$

These monotonicity conditions mean that Eqs 9–13 must be true

$$a_{\min} \geq d_{\max} \tag{9}$$
$$b_{\min} = 0 \tag{10}$$
$$c_{\min} = 0 \tag{11}$$
$$g_{\min} = 0 \tag{12}$$
$$\zeta_{\max,1} = b_{\max} v_r \tag{13}$$

3.2.2. Asymptotes conditions

Taking the limit of Eq 6 as $v \to \infty$ yields

$$\lim_{v\to\infty} q(\vec{\theta}, v) = a \tag{14}$$

Equation 14 is the exact value of the upper asymptote of Eq 6. However, in practice, $v < \infty$, but since we still want to help the STIR algorithm estimate a such that $q(\vec{\theta}, v)$ still fits the manufacturer-provided data well, we allow the value of a to vary within ±10% of P_r, resulting in the conditions

$$a_{\min} = 0.9P_r \tag{15}$$

$$a_{\max} = 1.1P_r \tag{16}$$

Equation 6 must be greater than 0 for all $v > 0$. Thus, $a - d$ must always be positive. This requires that

$$d_{\max} = 0 \tag{17}$$

Note that the conditions in Eqs 15 and 17 embody the condition in Eq 9.

3.2.3. Other limits

$\left[\frac{v}{c}\right]^{\zeta} \mathrm{e}^{-b\,(v\,-\,c)}$ in Eq 6 must start to substantially decrease at some point between v_{ci} and v_r. In other words, as v increases, $\left[\frac{v}{c}\right]^{\zeta} \mathrm{e}^{-b\,(v\,-\,c)}$ should become much smaller than one at some point between v_{ci} and v_r. Otherwise, the curve would never approach the upper asymptote (which is almost equal to P_r) when $v \to v_r$. Thus, the inflection point c must be somewhere between v_{ci} and v_r. We formulate the limits on c as follows

$$c_{\min} = v_{ci} \tag{18}$$

$$c_{\max} = v_r \tag{19}$$

Note that the condition in Eq 18 embodies the condition in Eq 11. $v_{\inf}$ (i.e., c) of an LF is the point at which a curve switches from concave upward to concave downward (i.e., the second derivative must be zero). Thus, taking the second derivative of Eq 6 with respect to v and equating it with zero

$$\frac{[\frac{v}{c}]^{\zeta}\mathrm{e}^{-b(v-c)}(-b^2v^2 + 2bv\zeta - \zeta^2 + \zeta)}{\left(1 + [\frac{v}{c}]^{\zeta}\mathrm{e}^{-b(v-c)}\right)^{g+1}} = -\frac{[\frac{v}{c}]^{2\zeta}\mathrm{e}^{-2b(v-c)}(\zeta - bv)^2(g+1)}{\left(1 + [\frac{v}{c}]^{\zeta}\mathrm{e}^{-b(v-c)}\right)^{g+2}} \tag{20}$$

Substituting $v = c$ in Eq 20 and simplifying

$$b^2c^2 + 2gbc\zeta + \zeta^2 = gb^2c^2 + 2bc\zeta + g\zeta^2 + 2\zeta \tag{21}$$

then solving Eq 21 for g as Eq 22

$$\begin{aligned} g &= \frac{\zeta^2 - 2bc\zeta + b^2c^2 - 2\zeta}{\zeta^2 - 2bc\zeta + b^2c^2} \\ &= 1 - \frac{2\zeta}{\zeta^2 - 2bc\zeta + b^2c^2} \end{aligned} \tag{22}$$

by taking the limits for various extreme values of ζ, we obtain Eq 23

$$\lim_{\zeta\to+\infty} g = 1 \quad \lim_{\zeta\to-\infty} g = 1 \quad \lim_{\zeta\to 0^+} g = 1 \quad \lim_{\zeta\to 0^-} g = 1 \tag{23}$$

this suggests that

$$g_{\max} = 1 \tag{24}$$

We solve Eq 22 for ζ

$$\zeta = \frac{1 + bc(1-g) + \sqrt{1 + 2bc(1-g)}}{1-g} \tag{25a}$$

$$\zeta = \frac{1 + bc(1-g) - \sqrt{1 + 2bc(1-g)}}{1-g} \tag{25b}$$

Equations 25a and 25b mean for every bc (the product of the two parameters) and g values, there are (in general) two ζ values to satisfy the condition $\left.\frac{d^2 q_e(\vec{\theta}, v)}{dv^2}\right|_{v=v_{\inf}} = 0$ (Eq 3). By plotting both equations in 3D for $g \sim [0, 0.95]$ and $bc \sim [0, 100]$, we see that the maximum value of ζ is 180. Thus, we say

$$\zeta_{\max,2} = 200 \tag{26}$$

Equations 13 and 26 dictate the upper limits for ζ to satisfy the monotonicity and the inflection point existence conditions, respectively. Since we must satisfy both conditions, it follows that

$$\zeta_{\max} = \text{minof}(\zeta_{\max,1}, \zeta_{\max,2}) = \text{minof}(b_{\max} v_r, 200) \tag{27}$$

where 'minof' means the minimum of the two choices.

3.3. Summary of the 6PLEZ LFs constraints

Equation 10, Eqs 12, 15–19 and 24 and 27 define nine constraints necessary for the STIR algorithm to quickly and reliably parameterize $\vec{\theta}$ in the 6PLEZ model (Eq 6). The three limits in which we did not derive analytically (or with reasoning) are: (1) $b_{\max}$ and (2) $d_{\min}$, (3) $\zeta_{\min}$.

We determined such limits by extensive simulations with the WT database of various ratings as follows: (1) $b_{\max} = 3$ and (2) $d_{\min} = -0.25\, P_r$, (3) $\zeta_{\min} = -500$. Table 2 shows a summary of the limits for the 6PLEZ logistic model.

Table 2. Constraints on the parameters of 6PLEZ logistic fit (Eq 6).

	Lower limits $\vec{\theta}_{\min}$		Upper limits $\vec{\theta}_{\max}$		How obtained
a	$0.9P_r$	Eq 15	$1.1P_r$	Eq 16	LL: analytically, UL: analytically
b	0	Eq 10	3		LL: analytically, UL: observation
c	v_{ci}	Eq 18	v_r	Eq 19	LL: proper reasoning, UL: proper reasoning
d	$-0.25P_r$		0	Eq 17	LL: observation, UL: analytically
g	0	Eq 12	1	Eq 24	LL: analytically, UL: analytically
ζ	−500			$\min(b_{\max}v_r, 200)$, Eq 27	LL: observation, UL: proper reasoning

Notice: LL: Lower Limit; UL: Upper Limit; $\vec{\theta}_{\min}$: a vector of minimum values for elements of $\vec{\theta}$; $\vec{\theta}_{\max}$: a vector of maximum values for elements of $\vec{\theta}$

3.4. Objective function definition

The main function to be minimized is the LSE between the fits of Eqs 4–6 and empirical power-speed data provided by the manufacturer. This is given as Eq 28:

$$f(\vec{\theta}_k) = \sum_{i=1}^{n} \left[q_e(\vec{\theta}_k,\, v_i) - q_m\,(v_i) \right]^2 \tag{28}$$

where $q_e(\vec{\theta}_k,\, v_i)$ are curves of Eqs 4–6; v_i, $q_m\,(v_i)$ are the i^{th} wind speed and wind power output data point as provided by the manufacturer, respectively; $\vec{\theta}_k$ is the parameters of vector θ in Eqs 4–6 at the k^{th} iteration; and n is the number of data points in the GCR (region between v_{ci} and v_r in Figure 1) as provided by the manufacturer. Aldaoudeyeh et al. [8] discussed further details on the application of STIR algorithm for WTPSC curve fitting.

Compared to other optimization algorithms, advantages of the STIR algorithm include: 1. an efficiency in solving large bound-constrained minimization problems [22, 23]; 2. An appeal for solving non-linear problems [22]; 3. An ability to handle convex, nonconvex, and ill-conditioned objective functions with large number of variables [24].

4. Results and discussion

We fit $\vec{\theta}$ parameters using STIR algorithm as described by Aldaoudeyeh et al. [8]. MAE, MAPE, RMSE and NRMSE as defined in [6, 25] are the statistical metrics we use to demonstrate the accuracy of our proposed model.

4.1. Accuracy near cut-in and rated wind speeds

To ensure as a fair comparison as possible, we compare our work to the closest one. Villanueva and Feijóo [19] provide fits for 6PL model (Eq 4) for multiple WTs. We choose four of them for comparison purposes: (1) Enercon E82 E2; (2) Repower MM82; (3) Siemens S82 SWT-2.3 82; (4) Vestas V164/8000.

Figure 5 shows curve fits for the 6PL model (as estimated by Villanueva and Feijóo [19]) and the 6PLEZ model (as estimated in this work). Although both models contain the same number of

parameters, our model (despite being a parametric one) fits the WTPSC curve near v_{ci} and v_r. Such inaccuracy is reported for LFs (see Yan et al. [20], for example), but it does not occur in our model.

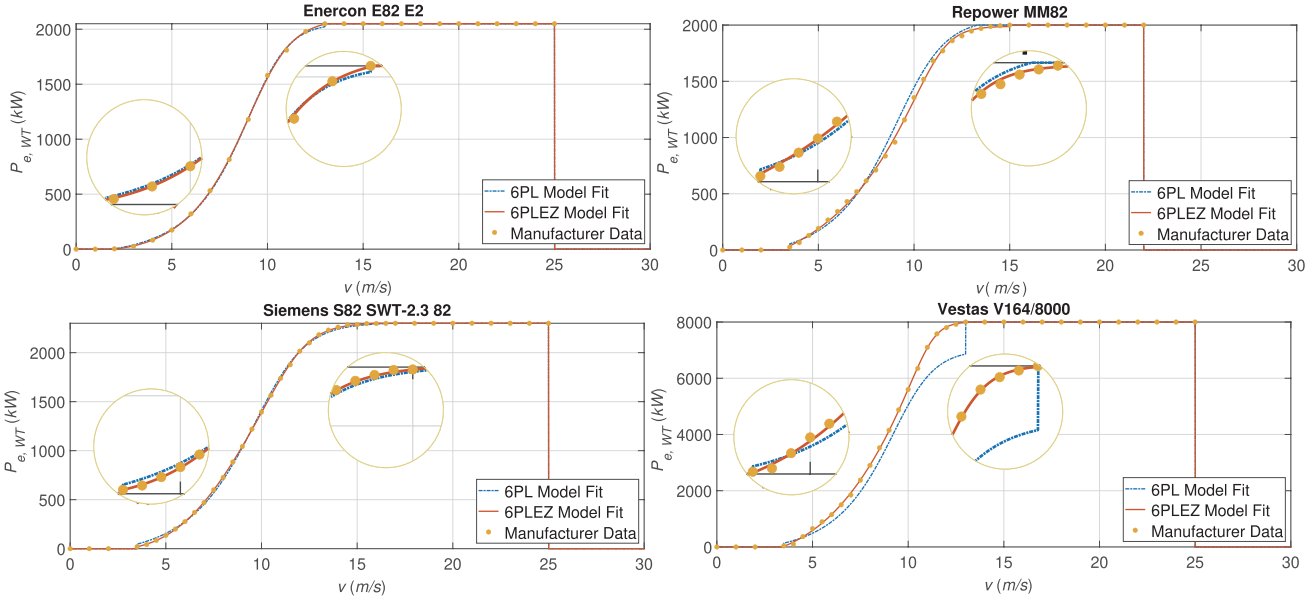

Figure 5. Comparison of fitting for 6PL and 6PLE models.

4.2. Benchmarking with WTs database

We test our model with 42 on-shore and off-shore WTs from 29 manufacturers. Ratings of the WTs range from 275 to 8000 kW. Tables 3 and 4 list the estimated $\vec{\theta}$ parameters, while Figures 6 and 7 show statistical metrics graphically. For convenience of presentation, we sorted WTs from with descending order of accuracy improvement. Clearly, the 6PLEZ model is either more accurate or at least as accurate as the 6PLE model.

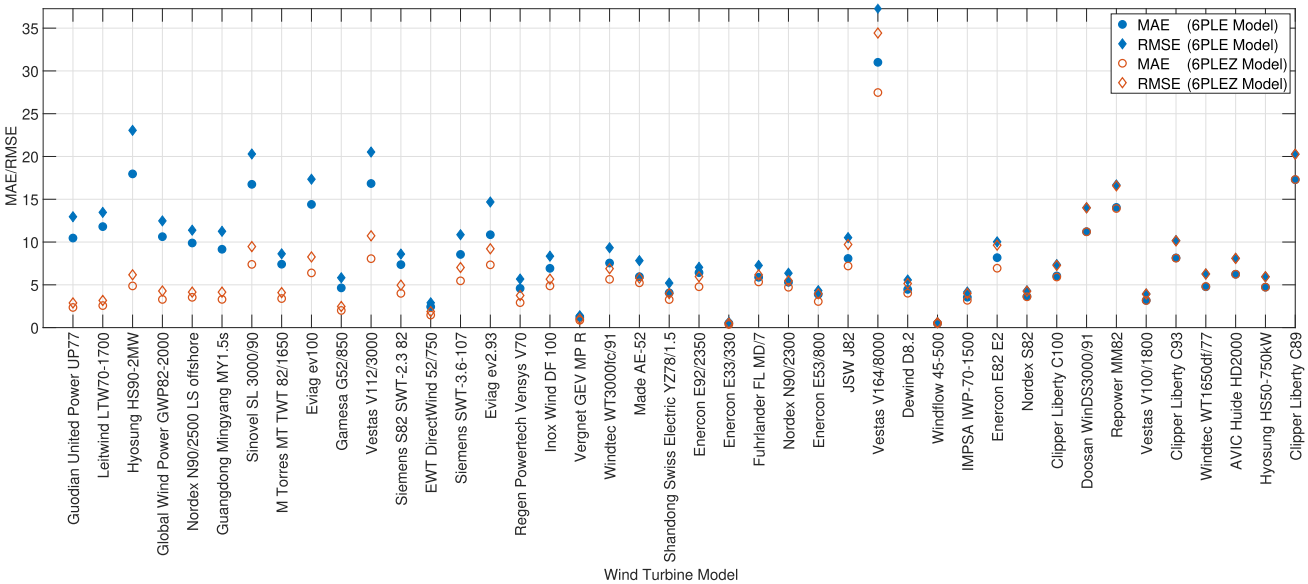

Figure 6. MAE and RMSE for 6PLEZ and 6PLE WTs logistic fits (Eq 6).

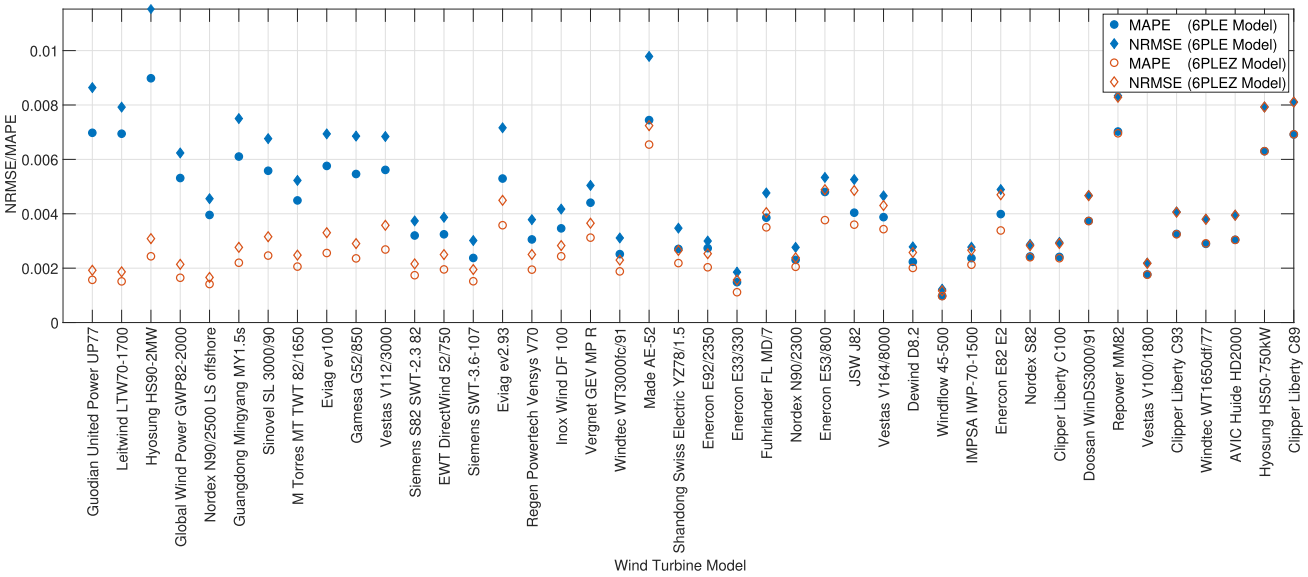

Figure 7. MAPE and NRMSE for 6PLE and 6PLEZ WTs logistic fits (Eqs 5 and 6).

Table 3. Parameters estimations for WTs of different ratings for the 6PLE model.

WT model	Rating (kW)	Estimated parameters					
		a	b	c	d	g	ε
Windtec WT1650df/77	1650	1576	1.615	10.24	−141.9	0.2114	0.7440
Windtec WT3000fc/91	3000	2866	1.227	11.46	−346.7	0.2175	0.6613
Windflow 45-500	500	492.3	1.313	10.42	−93.27	0.2258	0.9368
Vestas V100/1800	1800	1720	2.008	9.215	−408.7	0.1359	0.7640
Vestas V112/3000	3000	2934	0.8737	11.30	−306.0	0.3378	0.8916
Vestas V164/8000	8000	7636	1.778	10.88	−1290	0.1481	0.7417
Vergnet GEV MP R	275	264.6	0.9909	10.59	−33.34	0.3180	0.6362
Sinovel SL 3000/90	3000	2854	2.087	11.48	−426.8	0.1204	0.6230
Siemens S82 SWT-2.3 82	2300	2219	0.8866	10.94	−245.5	0.3493	0.8966
Siemens SWT-3.6-107	3600	3439	1.053	10.70	−389.9	0.2975	0.8619
Shandong Swiss Electric YZ78/1.5	1500	1426	2.783	9.826	−103.6	0.1308	0.6990
Repower MM82	2000	1928	1.413	11.17	−314.6	0.1712	0.8553
Regen Powertech Vensys V70	1500	1478	1.295	10.90	−116.4	0.2450	0.9323
Nordex S82	1500	1469	1.063	9.517	−182.0	0.3317	0.9083
Nordex N90/2500 LS offshore	2500	2420	1.126	10.77	−344.0	0.2439	0.8179
Nordex N90/2300	2300	2191	1.416	10.86	−519.4	0.1639	0.7269
Made AE-52	800	800.0	0.5824	9.994	−20.67	0.7892	0.6719
M Torres MT TWT 82/1650	1650	1630	0.7061	9.226	−127.8	0.5598	0.9359
Leitwind LTW70-1700	1700	1622	2.083	11.49	−154.5	0.1341	0.6356
JSW J82	2000	1898	1.600	11.23	−434.7	0.1321	0.6680
Inox Wind DF 100	2000	1896	1.783	8.547	−240.2	0.1932	0.6884
IMPSA IWP-70-1500	1500	1430	2.277	11.12	−189.9	0.1230	0.6919
Hyosung HS90-2MW	2000	1915	1.292	10.01	−193.7	0.2847	0.7484

Table 3 (continued)

WT model	Rating (kW)	Estimated parameters					
		a	b	c	d	g	ε
Hyosung HS50-750kW	750	715.3	3.427	11.30	−86.71	0.079 44	0.6020
Guodian United Power UP77	1500	1424	2.262	10.41	−203.4	0.1215	0.6182
Guangdong Mingyang MY1.5s	1500	1430	1.591	10.29	−140.7	0.2071	0.7068
Global Wind Power GWP82-2000	2000	1987	0.7925	10.25	−129.5	0.4587	0.9103
Gamesa G52/850	850	814.9	1.035	10.85	−123.6	0.2623	0.8458
Fuhrlander FL MD/7	1525	1490	1.079	10.27	−235.2	0.2643	0.8742
Eviag ev100	2500	2376	1.756	9.938	−227.4	0.1954	0.6965
Eviag ev2.93	2050	2003	0.9065	9.172	−134.4	0.5021	0.8590
Enercon E92/2350	2350	2345	0.9208	9.526	−76.27	0.5096	0.9880
Enercon E82 E2	2050	2016	0.9338	9.669	−66.77	0.4910	0.9254
Enercon E33/330	335	332.4	0.7343	9.298	−12.29	0.6540	0.9220
Enercon E53/800	810	788.1	1.179	9.874	−37.54	0.3385	0.9183
EWT DirectWind 52/750	750	739.1	0.9819	10.15	−44.36	0.3776	0.9304
Doosan WinDS3000/91	3000	2870	1.759	10.92	−77.35	0.2260	0.8047
Dewind D8.2	2000	1994	0.7215	7.917	−114.9	0.8369	0.8851
Clipper Liberty C93	2500	2436	1.249	10.76	−244.9	0.2505	0.9016
Clipper Liberty C100	2500	2480	1.099	10.22	−235.1	0.3076	0.9526
Clipper Liberty C89	2500	2447	1.173	10.81	−93.36	0.3307	0.9347
AVIC Huide HD2000	2050	1957	1.674	9.901	−258.7	0.1947	0.7736

Table 4. Parameters estimations for WTs of different ratings for the 6PLEZ model.

WT model	Rating (kW)	Estimated parameters					
		a	b	c	d	g	ζ
Windtec WT1650df/77	1650	1686	1.750	10.42	−175.5	0.2082	1.406
Windtec WT3000fc/91	3000	3107	0.018 57	12.15	−46.62	0.1391	−19.87
Windflow 45-500	500	501.3	0.5517	10.64	−45.75	0.2094	−8.888
Vestas V100/1800	1800	1799	1.833	9.354	−343.6	0.1394	−1.672
Vestas V112/3000	3000	3005	0	13.33	30.21	0.048 14	−126.8
Vestas V164/8000	8000	8015	0.3718	11.24	−365.5	0.1215	−19.24
Vergnet GEV MP R	275	282.8	0	11.62	−6.191	0.083 86	−49.43
Sinovel SL 3000/90	3000	2999	0	12.02	−9.974	0.043 48	−92.05
Siemens S82 SWT-2.3 82	2300	2319	0	12.47	−16.08	0.1377	−36.09
Siemens SWT-3.6-107	3600	3613	0	11.62	−47.49	0.1707	−23.59
Shandong Swiss Electric YZ78/1.5	1500	1498	1.343	10.05	−19.66	0.1096	−18.46
Repower MM82	2000	1989	1.264	11.30	−242.6	0.1747	−1.768
Regen Powertech Vensys V70	1500	1503	0.091 58	11.36	−13.24	0.1722	−16.39
Nordex S82	1500	1525	0.2547	10.01	−65.12	0.2620	−9.131
Nordex N90/2500 LS offshore	2500	2526	0	11.74	−36.94	0.1087	−36.07

Table 4 (continued)

WT model	Rating (kW)	Estimated parameters					
		a	b	c	d	g	ζ
Nordex N90/2300	2300	2328	0	11.38	−128.3	0.1323	−20.00
Made AE-52	800	800.3	0	11.71	13.59	0.013 53	−374.9
M Torres MT TWT 82/1650	1650	1693	0	12.31	1.248	0.080 53	−65.60
Leitwind LTW70-1700	1700	1701	0	12.03	4.671	0.037 13	−101.4
JSW J82	2000	2019	0.2879	11.67	−98.75	0.1174	−17.89
Inox Wind DF 100	2000	2027	0	9.076	−13.55	0.1121	−28.12
IMPSA IWP-70-1500	1500	1505	1.463	11.33	−88.78	0.1188	−10.56
Hyosung HS90-2MW	2000	2000	0	11.10	2.642	0.021 19	−318.6
Hyosung HS50-750kW	750	748.3	3.388	11.45	−84.47	0.079 69	−0.4132
Guodian United Power UP77	1500	1499	0	10.95	−10.07	0.034 76	−111.0
Guangdong Mingyang MY1.5s	1500	1503	0	11.02	−9.377	0.056 91	−77.47
Global Wind Power GWP82-2000	2000	2036	0	12.10	−5.765	0.1168	−38.87
Gamesa G52/850	850	850.0	0	12.86	14.89	0.024 16	−278.7
Fuhrlander FL MD/7	1525	1547	0	11.27	−24.56	0.1325	−31.33
Eviag ev100	2500	2507	0	10.55	−14.82	0.073 18	−55.92
Eviag ev2.93	2050	2055	0	11.20	23.19	0.033 25	−227.5
Enercon E92/2350	2350	2361	0.3550	10.08	−14.94	0.3588	−6.829
Enercon E82 E2	2050	2096	0.4879	10.18	−17.17	0.3736	−5.488
Enercon E33/330	335	352.4	0.1004	10.38	−1.293	0.3939	−7.691
Enercon E53/800	810	811.2	0.4786	10.29	−6.623	0.2568	−8.688
EWT DirectWind 52/750	750	758.6	0	10.96	−5.549	0.2220	−13.92
Doosan WinDS3000/91	3000	3019	1.822	11.04	−91.61	0.2271	0.7850
Dewind D8.2	2000	2200	0	10.89	−12.30	0.1473	−44.29
Clipper Liberty C93	2500	2507	1.128	10.87	−194.4	0.2501	−1.414
Clipper Liberty C100	2500	2522	0.3279	10.61	−61.88	0.2478	−9.311
Clipper Liberty C89	2500	2505	1.173	10.87	−93.22	0.3308	0.001 366
AVIC Huide HD2000	2050	2071	1.633	10.06	−245.6	0.1954	−0.4215

Table 6 shows four statistical metrics (MAE, RMSE, MAPE, and NRMSE) with their mean, median, maximum and minimum values for the entire database of WTs. Villanueva and Feijóo [21] provided classifications of the accuracy of WTPSC models depending on MAPE values. Such categories are summarized in Table 5. Tables 5 and 6 show that: (1) Both mean and median MAPE values for the 6PLE and 6PLEZ models fall in the 'very high' category. However, the 6PLEZ model has a median MAPE of 0.002383, which is less than half the 'very high' category threshold and (2) both mean and median NRMSE for the 6PLEZ model are 32.3 % and 38.5 % less than for the 6PLE model. This is a substantial accuracy improvement while maintaining the same number of parameters.

Table 5. Classifications of WTPSC accuracy levels.

Accuracy level	MAPE range
Very high	< 0.005
High	0.005–0.025
Medium	0.025–0.1
Low	0.1–0.15

Table 6. Statistical metrics for 6PLE and 6PLEZ logistic fits (Eqs 5 and 6).

	Mean	Median	Max	Min
	MAE			
6PLE	8.250	7.145	31.01	489.6×10^{-3}
6PLEZ	5.577	4.751	27.47	0.3737
	RMSE			
6PLE	10.07	8.470	37.27	613.1×10^{-3}
6PLEZ	6.949	5.570	34.43	0.5241
	MAPE			
6PLE	4.175×10^{-3}	3.866×10^{-3}	8.983×10^{-3}	9.791×10^{-4}
6PLEZ	2.782×10^{-3}	2.383×10^{-3}	6.959×10^{-3}	9.721×10^{-4}
	NRMSE			
6PLE	5.103×10^{-3}	4.666×10^{-3}	1.153×10^{-3}	1.226×10^{-3}
6PLEZ	3.452×10^{-3}	2.866×10^{-3}	8.285×10^{-3}	1.165×10^{-3}

5. Final remarks, limitations and recommendations

One limitation of the study is the use of manufacturer-provided data. Because of several factors (e.g., wind power curtailment, accumulation of dirt and snow, sensor failures, and pitch angle control malfunctioning [26–28]), the real power-speed data points may not be exactly the same as the ones provided by the manufacturer. In short, the data was characterized by noise and outliers. According to the IEC 61400-12-1 standard, outliers are highly weighted by the ordinary LSE regression method [29]. This conclusion should also pertain to most WTPSC fitting methods, as virtually all of them employ the LSE as an objective function. Pei and Li [11] confirm that outliers compromise the accuracy machine-learning WTPSC fitting methods.

When fitting using the manufacturer datasheet, the data points were obtained under controlled conditions. For example, the air mass density was set to $1.225\,\mathrm{kg\,m^{-3}}$, the wake effect was neglected (because only one WT was tested at a time), and the TI was assumed to be 10 % [30]. The conditions in the actual WT location are usually not the same. The implementation of test condition control promoted fairness in comparing different WTPSC fitting models or estimation methods.

When fitting with real power-speed data, the air mass and TI may fluctuate for similar wind speed measurements, while the wake effect was greatly affected by the distance between WTs and their yaw angles. Additionally, several data cleaning techniques were devised in the literature (see [6, 20, 31]),

which could be incorporated in future research. The amount of data we must remove, however, changes depends on the WT itself, making the entire data cleaning process susceptible to subjectivity [32], and sometimes outliers may still be present in the processed data [28].

In summary, although many papers addressed the effect of outliers on the accuracy of WTPSC models and the sensitivity of their parameters (e.g., [32, 33]), the literature contained only few for LFs WTPSC models and most of them were in the last five years (e.g., [11, 18, 20]). Bilendo et al. [31] provide a recent review of WTPSC, but with no conclusive remarks on the effect of outliers on the performance of LFs WTPSC models. Thus, we suggest the following as future work:

1. Development of new robust LFs WTPSC curve fitting techniques (or objective functions) to guarantee model resiliency against outliers;

2. Incorporating additional parameters into the model to account for typical factors affecting outliers;

3. Examining the correlation between data filtering techniques and criteria and the accuracy of LFs WTPSC modeling;

4. Formulating probabilistic LFs WTPSC curves to accommodate fluctuations in instantaneous turbulence in wind speeds or enhanced LFs WTPSC to guarantee that the 10-minute averaged power closely approximates the empirical data.

6. Conclusions

In this paper, we proposed the 6PLEZ model (Eq 6). We then derived upper and lower limits for its parameters (Table 2) and estimated them using the STIR algorithm. The significance of this paper is:

1. Our model adapts to improving accuracy in some WTPSC regions without sacrificing the accuracy in others (SubSection 3.1);

2. Unlike most parametric approaches, the 6PLEZ model provides accurate WTPSC modeling near v_{ci} and v_r (SubSection 4.1);

3. The limits on the parameters of the 6PLEZ model are clearly specified, which:

   (a) guarantee the monotonicity of the model (Eq 8);

   (b) provide robust and reliable estimation of the parameters with no difficulties in 'guessing' their range (Table 2);

4. It provides substantial accuracy improvement over the 6PLE model despite having the same number of parameters as the 6PL and 6PLE models (Tables 5 and 6).

Use of AI tools declaration

The authors declare they have not used Artificial Intelligence (AI) tools in the creation of this article.

Conflict of interest

The authors declare that they have no known competing financial interests or personal relationships that could have appeared to influence the work reported in this paper.

References

1. Global Wind Energy Council (2021) *Global wind report 2021*, Brussels: Global Wind Energy Council, 6–7.
2. Willis DJ, Niezrecki C, Kuchma D, et al. (2018) Wind energy research: State-of-the-art and future research directions. *Renewable Energy* 125: 133–154. https://doi.org/10.1016/j.renene.2018.02.049
3. Hitaj C, Löschel A (2019) The impact of a feed-in tariff on wind power development in germany. *Resour Energy Econ* 57: 18–35. https://doi.org/10.1016/j.reseneeco.2018.12.001
4. Lin BQ, Chen YF (2019) Impacts of policies on innovation in wind power technologies in China. *Appl Energy* 247: 682–691. https://doi.org/10.1016/j.apenergy.2019.04.044
5. Al Motasem IA, Alzaareer K (2020) Evaluating the accuracy of wind turbine power-speed characteristics fits for the generator control region. *Int J Renewable Energy Res* 10: 1031–1041. https://doi.org/10.20508/ijrer.v10i2.10955.g7975
6. Hu Y , Xi YH , Pan CY, et al. (2020) Daily condition monitoring of grid-connected wind turbine via high-fidelity power curve and its comprehensive rating. *Renewable Energy* 146: 2095–2111. https://doi.org/10.1016/j.renene.2019.08.043
7. Shokrzadeh S, Jozani MJ, Bibeau E (2014) Wind turbine power curve modeling using advanced parametric and nonparametric methods. *IEEE Trans Sustainable Energy* 5: 1262–1269. https://doi.org/10.1109/TSTE.2014.2345059
8. Aldaoudeyeh AM, Alzaareer K, Harasis S, et al. (2021) A new method to fit logistic functions with wind turbines power curves using manufacturer datasheets. *IET Renewable Power Gener* 16: 287–299. https://doi.org/10.1049/rpg2.12309
9. Sohoni V, Gupta SC, Nema RK (2016) A critical review on wind turbine power curve modelling techniques and their applications in wind based energy systems. *J Energy* 2016: 1–18. https://doi.org/10.1155/2016/8519785
10. Aldaoudeyeh AMI, Alzaareer K (2020) Statistical analysis of wind power using weibull distribution to maximize energy yield. *2020 IEEE PES/IAS PowerAfrica* 2020: 1–5.
11. Pei S, Li Y (2019) Wind turbine power curve modeling with a hybrid machine learning technique. *Appl Sci* 9: 4930. https://doi.org/10.3390/app9224930
12. Kawano T, Wallbridge N, Plummer C (2020) Logistic models for simulating the growth of plants by defining the maximum plant size as the limit of information flow. *Plant Signaling Behav* 15: 1709718. https://doi.org/10.1080/15592324.2019.1709718
13. Rahimi I, Chen F, Gandomi AH (2021) A review on covid-19 forecasting models. *Neural Comput Appl* 35: 23671–23681. https://doi.org/10.1007/s00521-020-05626-8

14. Al-Hinai A, Charabi Y, Aghay Kaboli SH (2021) Offshore wind energy resource assessment across the territory of oman: A spatial-temporal data analysis. *Sustainability* 13: 2862. https://doi.org/10.3390/su13052862

15. Lydia M, Selvakumar AI, Kumar SS, et al. (2013) Advanced algorithms for wind turbine power curve modeling. *IEEE Trans Sustainable Energy* 4: 827–835. https://doi.org/10.1109/TSTE.2013.2247641

16. Taslimi-Renani E, Modiri-Delshad M, Elias MFM, et al. (2016) Development of an enhanced parametric model for wind turbine power curve. *Appl Energy* 177: 544–552. https://doi.org/10.1016/j.apenergy.2016.05.124

17. Zou R, Yang J, Wang Y, et al. (2021) Wind turbine power curve modeling using an asymmetric error characteristic-based loss function and a hybrid intelligent optimizer. *Appl Energy* 304: 117707. https://doi.org/10.1016/j.apenergy.2021.117707

18. Jing B, Qian Z, Zareipour H, et al. (2021) Wind turbine power curve modelling with logistic functions based on quantile regression. *Appl Sci* 11: 3048. https://doi.org/10.3390/app11073048

19. Villanueva D, Feijóo A (2018) Comparison of logistic functions for modeling wind turbine power curves. *Electr Power Syst Res* 155: 281–288. https://doi.org/10.1016/j.epsr.2017.10.028

20. Yan J, Zhang H, Liu Y, et al. (2019) Uncertainty estimation for wind energy conversion by probabilistic wind turbine power curve modelling. *Appl Energy* 239: 1356–1370. https://doi.org/10.1016/j.apenergy.2019.01.180

21. Villanueva D, Feijóo A (2020) A review on wind turbine deterministic power curve models. *Appl Sci* 10: 4186. https://doi.org/10.3390/app10124186

22. Branch MA, Coleman TF, Li Y (1999) A subspace, interior, and conjugate gradient method for large-scale bound-constrained minimization problems. *SIAM J Sci Comput* 21: 1–23. https://doi.org/10.1137/S1064827595289108

23. Conn AR, Gould NIM, Toint PL (1998) Global convergence of a class of trust region algorithms for optimization with simple bounds. *SIAM J Numer Anal* 25: 433–460. https://doi.org/10.1137/0725029

24. Kamandi A, Amini K, Ahookhosh M (2016) An improved adaptive trust-region algorithm. *Optim Lett* 11: 555–569. https://doi.org/10.1007/s11590-016-1018-4

25. Villanueva D, Feijóo AE (2016) Reformulation of parameters of the logistic function applied to power curves of wind turbines. *Electr Power Syst Res* 137: 51–58. https://doi.org/10.1016/j.epsr.2016.03.045

26. Lapira E, Brisset D, Ardakani HD, et al. (2012) Wind turbine performance assessment using multi-regime modeling approach. *Renewable Energy* 45: 86–95. https://doi.org/10.1016/j.renene.2012.02.018

27. Lin Z, Liu X (2020) Wind power forecasting of an offshore wind turbine based on high-frequency scada data and deep learning neural network. *Energy* 201: 117693. https://doi.org/10.1016/j.energy.2020.117693

28. Wang Y, Hu Q, Li L, et al. (2019) Approaches to wind power curve modeling: A review and discussion. *Renewable Sustainable Energy Rev* 116: 109422. https://doi.org/10.1016/j.rser.2019.109422

29. International Electrotechnical Commission (2007) Wind energy generation systems—Part 12-1: Power performance measurements of electricity producing wind turbines. International Electrotechnical Commission (IEC), IEC Central Office, 3: 2017-03.

30. Sunderland K, Woolmington T, Blackledge J, et al. (2013) Small wind turbines in turbulent (urban) environments: A consideration of normal and weibull distributions for power prediction. *J Wind Eng Ind Aerodyn* 121: 70–81. https://doi.org/10.1016/j.jweia.2013.08.001

31. Bilendo F, Meyer A, Badihi H, et al. (2022) Applications and modeling techniques of wind turbine power curve for wind farms—A review. *Energies* 16: 180. https://doi.org/10.3390/en16010180

32. Mehrjoo M, Jozani MJ, Pawlak M (2020) Wind turbine power curve modeling for reliable power prediction using monotonic regression. *Renewable Energy* 147: 214–222. https://doi.org/10.1016/j.renene.2019.08.060

33. Pelletier F, Masson C, Tahan A (2016) Wind turbine power curve modelling using artificial neural network. *Renewable Energy* 89: 207–214. https://doi.org/10.1016/j.renene.2015.11.065

AIMS Press